Use of wavefront encoding in optical interconnects and fiber switches for cross talk mitigation

Brian Robertson,[1,2] Zichen Zhang,[1] Maura M. Redmond,[1] Neil Collings,[1] Jinsong Liu,[1] R. S. Lin,[1] Anna M. Jeziorska-Chapman,[1] John R. Moore,[1] William A. Crossland,[1] and D. P. Chu[1,3]

[1]Photonics and Sensors Group, Department of Engineering, University of Cambridge, 9 JJ Thomson Avenue, CB3 0FA, Cambridge,UK

[2]br249@cam.ac.uk

[3]dpc31@cam.ac.uk

Received 18 August 2011; accepted 21 September 2011; posted 21 October 2011 (Doc. ID 153072); published 10 February 2012

A technique of cross talk mitigation developed for liquid crystal on silicon spatial light modulator based optical interconnects and fiber switches is demonstrated. By purposefully introducing an appropriate aberration into the system, it is possible to reduce the worst-case cross talk by over 10 dB compared to conventional Fourier-transform-based designs. Tests at a wavelength of 674 nm validate this approach, and show that there is no noticeable reduction in diffraction efficiency. A 27% spot increase in beam diameter is observed, which is predicted to reduce at longer datacom and telecom wavelengths.

OCIS codes: 070.6120, 060.6718, 090.0090, 200.4650.

1. Introduction

Low cross talk fiber switches and reconfigurable optical interconnects play key roles in optical communication networks and computer systems. Several approaches for implementing such modules have been proposed, including those utilizing microelectromechanical systems [1,2] and liquid-crystal-on-silicon (LCOS) phase-only spatial light modulators (SLMs) [3,4]. Previous work in the field of LCOS switches has concentrated on the use of gratings [3–6]. Although these switches have many advantages, including the ability to fine-tune alignment [7], and lower sensitivity to pixel failure, we always observe higher diffraction orders due to spatial and phase quantization [8,9], and, more importantly, the problems involved with LCOS SLM display errors, such as temporal instabilities, pixel edge effects [10], and spatial nonuniformities. As a result, the actual and required phase patterns may deviate to such an extent that unacceptable interchannel cross talk occurs.

Cross talk mitigation in LCOS-based fiber switches has been previously investigated by several groups. For example, in the case of the ROSES project [3] and subsequent work by Uche *et al.* [4] the symmetry of the spatial positions of the output ports was broken to minimize cross talk. In this paper we discuss an alternative use of broken symmetry to negate cross talk, which we refer to as wavefront encoding. The approach involves purposefully building an aberration into the layout of the optical system, such as defocus, which must be corrected by the SLM to ensure optimal coupling into an output detector or fiber. In the case where we route to a certain output port, this correction is valid for only one diffraction order, with the aberrations increasing for the other orders. As a result the amount of cross talk light coupled to the other output positions can be reduced. In previous work, Neil *et al.* [11] demonstrated how a binary diffractive element can be used to arbitrarily

1559-128X/12/050659-10$15.00/0

aberrate different diffraction orders. A similar approach was used by Gil Leyva *et al.* [12] for aberration analysis and corrections in a free-space optical interconnect, a technique which was described as also having the potential for cross talk control. We show how cross talk can be reduced in a fiber switch or free-space reconfigurable interconnect based on one of the simplest aberrations, defocus. It may indeed be possible to reduce cross talk in a switch by carefully offsetting the zeroth order from the output fiber array, either by tilting the SLM, or by translating the Fourier transform lens. The periodicity of the diffraction orders at the replay plane would therefore be, hopefully, incommensurate to the periodicity of the fibers, and as a result, only the $+1$ order would couple efficiently into an output port. This approach can work to a certain extent if all the focused cross talk beams fall between the fibers and the fibers are spaced well apart in between (much larger than the focused beam spot size). Moreover, if lenslet arrays are used to couple light into the fibers, the offset cross talk beams may still be partially focused into the output ports. Finally, it should be stressed that the approach described in this paper has the potential of being extended to astigmatism in switches that use cylindrical optics, and to more complex wavefront distortions that use an array of diffractive filters incorporated with lenslet arrays placed before the fiber to discriminate between signals. A more generalized approach of wavefront encoding will be discussed at a later date.

Figure 1 illustrates how wavefront encoding based on defocusing can be applied to a fiber switch. The $2f$ optical arrangement of Fig. 1(a) consists of an input/output fiber array positioned at plane F_1, a reflective LCOS SLM, and a Fourier transform lens of focal length f. The input signal of wavelength λ, launched into the system via the central fiber, is collimated, and is then incident on the SLM where a quantized phase-only blazed grating of period T is displayed. The incident beam is diffracted into a number of orders, which are focused at plane Q_1. The power in each order, P_m, is dependent on the exact nature of the phase pattern. In the case of the mth order, the diffraction angle, θ_m, is given by

$$\sin(\theta_m) = \frac{m\lambda}{T}. \tag{1}$$

The corresponding paraxial position of the diffraction order, δ_m, at plane Q_1 is thus

$$\delta_m = f \tan(\theta_m). \tag{2}$$

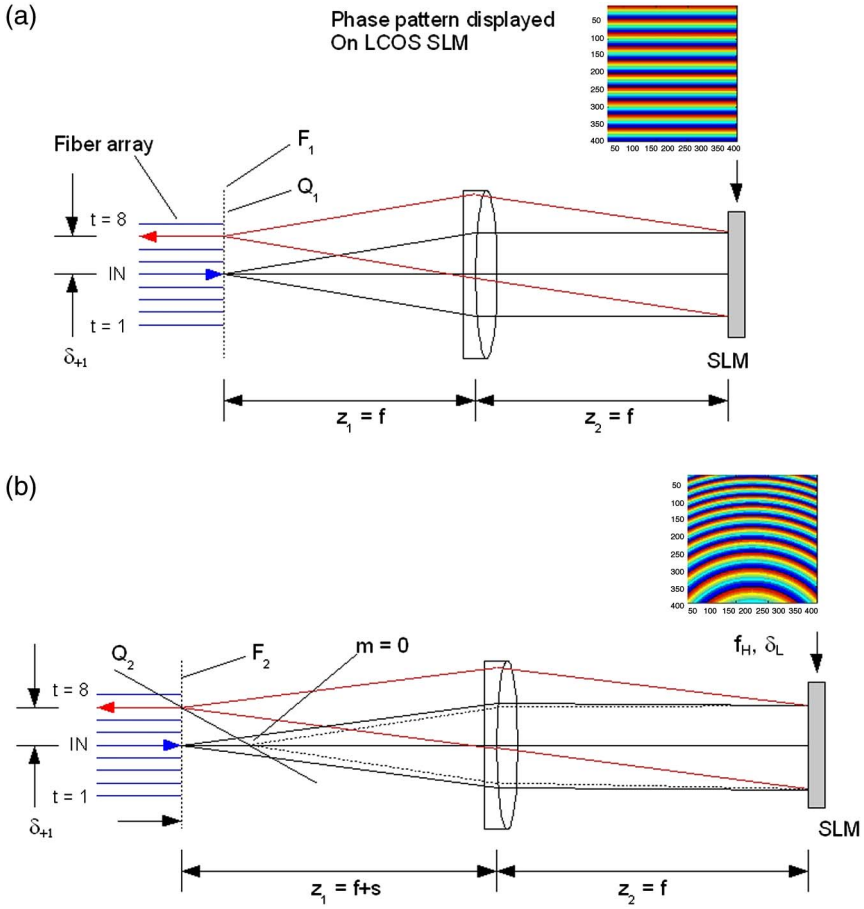

Fig. 1. (Color online) Experimental outline of wavefront encoding as applied to a $4f$ optical routing geometry. (a) Perfectly aligned system. (b) Defocused system.

Because of the symmetry of this system, planes Q_1 and F_1 coincide, and the focused beams have the same spot profile, though different peak intensities. This can lead to cross talk; if we aim to direct the $+1$ order to one of the output fibers, light remaining in other orders may couple into one or more of the other fibers. To minimize this problem we purposefully move the fiber array a distance s from plane F_1 to plane F_2, and replace the grating with an offset holographic lens to refocus for the target output fiber only. As shown by Blanchard and Greenaway [13], such a defocus-grating-lens results in the diffraction orders being focused at different planes. Thus, if we optimize the SLM pattern such that the $+1$ order is focused at plane F_2, we will only obtain optimum coupling efficiency for that order; all other orders are focused on a new surface, Q_2, which is no longer coplanar with respect to F_2, hence the reduced cross talk for other output fibers on that plane.

2. Theory of Wavefront Encoding Based on Defocus

This section develops a model for the LCOS-SLM-based switch illustrated in Fig. 1(b), where the introduced aberration is a simple defocus of value s. We shall then use a commercial optical design package to relate the relative coupling efficiencies of the SLM diffraction orders to this defocus. It will be assumed that the SLM displays an off-axis holographic lens to optimally couple the $m = +1$ diffraction order to the required output fiber. Thus the cross talk in such a switch depends on two factors: the power in each specific order, P_m, which is determined by the limitations of the SLM in displaying the optimum phase pattern, and the relative defocus of each order with respect to the fiber plane, which affects the coupling efficiency of that order, $\eta(m)$. We shall investigate the latter factor—how defocus relates to coupled power.

It shall be assumed that standard single-mode telecom fibers are used in the switches of Fig. 1, with a mode field radius, w_f, of $5.2\,\mu$m at 1550 nm. If the SLM displays an off-axis holographic lens of focal length f_H that is offset from the optical axis by δ_H instead of a blazed grating, the diffraction orders will be focused at different distances, $d(m)$, with respect to the fiber plane, where m is the order number. The coupling efficiency of a specific order as a function of defocus, $d(m)$, can therefore be calculated to a first approximation by evaluating the mode overlap integral of the resultant output waist, $w(m)$, and a single-mode fiber that is longitudinally shifted from the beam waist by $d(m)$ [14]. This is the approach we shall use to determine the optimum value for f_H for our switch geometry.

Equations (1) and (2) relate the deflection distance of the $+1$ order, δ_{+1}, to the period of the periodic grating of Fig. 1(a). Unfortunately, there are a number of limitations that restrict the usable deflection range in such a system related to the finite SLM pixel size, Δ, the number of phase levels used, q, and the number of pixels illuminated, N_{SLM}. These have been discussed in detail by several authors [5,8,9, and 15]. Their studies have shown that although the maximum deflection angle occurs when the period $T = 2\Delta$, the usable deflection angles are restricted to a smaller range due to a roll-off in diffraction efficiency that occurs when a quantized blazed grating is displayed on the SLM [15]. In addition, the number of individually addressable points at the replay plane is directly proportional to the number of SLM pixels illuminated. As a result, in order to maximize the number of output ports in the switch while matching the performance of currently available LCOS SLMs in terms of pixel size and pixel count, it is necessary to either use an intermediate lenslet array or bring the fibers closer together using a waveguide concentrator element to match the deflection capabilities of the SLM to the $250\,\mu$m spacing of a standard fiber ribbon. For this analysis we shall consider the latter case, and use the geometry of the ROSES switch [3] as the starting point for a wavefront-encoded geometry. The ROSES switch used a waveguide component to convert the standard $250\,\mu$m pitch of a fiber ribbon down to approximately $35\,\mu$m. However, as mentioned in the introduction the ports were positioned nonuniformly to reduce cross talk. The switch analyzed in this section will assume a similar technique to reduce the input port pitch, but with the port spacing set uniformly at $35\,\mu$m, and wavefront encoding used to mitigate cross talk. We shall consider eight output ports arranged symmetrically about the input with a mode field radius of $5.2\,\mu$m, a doublet of 25 mm focal length, an SLM pixel size $\Delta = 15\ \mu$m, and target the minimum period to be greater than 8Δ to maximize diffraction efficiency. The target positions are therefore $\delta_{+1} = \pm 35, \pm 70, \pm 105$, and $\pm 140\ \mu$m, respectively.

Figure 1(b) shows a switch where the SLM displays a holographic lens of focal length f_H, offset from the optical axis by δ_H. Ideally all the light is diffracted by the SLM into the $+1$ order; however, a certain amount of light is diffracted into the other orders. The mth order appears diffracted by a lens of focal length $f_H(m)$, where

$$f_H(m) = \frac{f_H}{m}. \tag{3}$$

As we are assuming the off-axis lenses are imperfect due to SLM limitations, we shall consider all orders, $m = 0, \pm 1, \pm 2, \pm 3\ldots$. Note that when $m = 0$, the focal length of the holographic lens is infinite, thus the light is not focused for this order. With reference to Fig. 1(b), if $z_2 = f$, we can show using paraxial theory that the defocus of the mth order, $d(m)$, with respect to the fiber plane is given by

$$d(m) = 2s + \frac{f^2}{f_H} m, \tag{4}$$

where the condition that the $m = +1$ order is focused at the output fiber plane for a given defocus value of s is

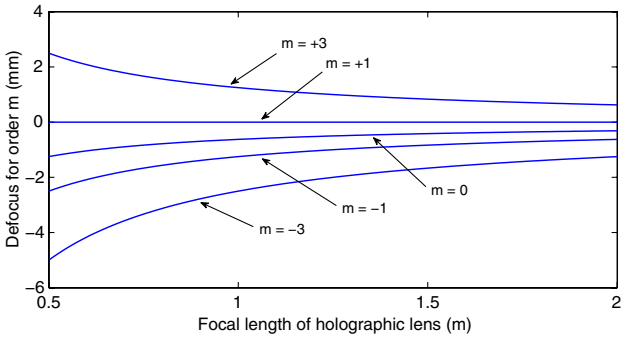

Fig. 2. (Color online) Defocus for the specified orders as a function of $f_H(+1)$. Lens focal length is $f = 25$ mm.

$$f_H = -\frac{f^2}{2s}. \tag{5}$$

To analytically determine the percentage of power in the mth order that is coupled into an output port, $\eta(m)$, we can apply Gaussian beam propagation theory and a mode overlap integral. Such a calculation was performed for an on-axis diffractive lens system assuming a 25 mm focal length lens and an input/output mode field radius of 5.2 μm at 1550 nm. Figure 2 shows the defocus, $d(m)$, for the orders $m = 0, \pm 1$, and ± 3 as $f_H(+1)$ is varied from 0.5 to 2.0 m [calculated using Eqs. (4) and (5)]. Note that a similar response would be obtained if the focal length were varied from −0.5 to −2.0 m. Figure 3 gives the corresponding variation in coupling efficiency. For the $m = +1$ order, the efficiency is 100% for all values of $f_H(+1)$, and the $m = 0$ and $m = +3$ curves overlap. The coupling efficiency for the other orders decrease with decreasing holographic lens focal length until they are down by over 2 orders of magnitude when $f_H(+1) = 0.5$ m. However, to calculate the actual cross talk we must also include the relative optical power in that order. Let us assume that the target port is located at position (x_t, y_t), and the mth order is centered at (x_m, y_m), the cross talk power coupled into the tth fiber by the mth order, $\mathrm{PC}(m,t)$, can be obtained by multiplying the power in the mth diffraction order, P_m, by the percentage of this power coupled into the tth fiber:

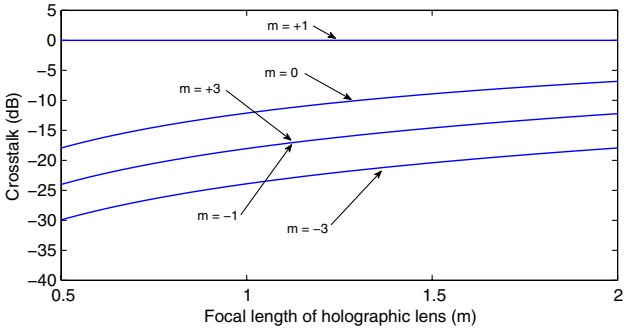

Fig. 3. (Color online) Coupling efficiency plot for the specified orders as a function of $f_H(+1)$. Note that the $m = -1$ and $m = +3$ orders overlap.

$$\mathrm{PC}(m,t) = P_m \eta(d(m), x_m - x_t, y_m - y_t). \tag{6}$$

The actual power term, P_m, depends on the accuracy that the desired phase profile is displayed, and is a complex interplay between spatial and phase quantization, temporal effects, liquid crystal properties, and field fringing effects. However, the advantage of wavefront encoding based on defocus is that these factors are less important due to the fact that the coupling efficiency is only maximized for the $m = +1$ order.

By the application of geometric optical theory the position of the +1 beam at the fiber plane, δ_{+1}, as a function of off-axis lens offset, δ_H, can be shown to be

$$\delta_{+1} = \frac{2s}{f}\delta_H. \tag{7}$$

Thus there is a linear relationship between the holographic lens offset and the signal beam position that is dependant only on the focal length of the focusing lens, f, and the defocus, s.

One of the drawbacks associated with using quantized holographic lenses based on a pixelated SLM is that the minimum local period [16] of pixels decreases with decreasing holographic lens focal length and increasing lens offset. Thus, eventually the number of pixels appearing in those lens segments close to the lens edge will be reduced to such a level that the local diffraction efficiency will roll-off and apodize the diffracted beam. Several groups have investigated this quantization effect for both static diffractive optical elements and dynamic SLM lenses [17]. Thus there is a trade-off between defocus and the required maximum offset δ_{+1}. This is illustrated in Fig. 4 where we assume that the SLM covers 500 × 500 pixels with a pixel size of 15 μm, the operating wavelength is 1550 nm, and the lens offset, δ_H, is 0, 1, 2, 3, 4, 5, and 6 mm.

Based on the above calculations, we shall choose a focal length of −1.0 m as this allows us to meet the 8 pixel minimum period limit at an operating wavelength of 1550 nm across all eight output ports where

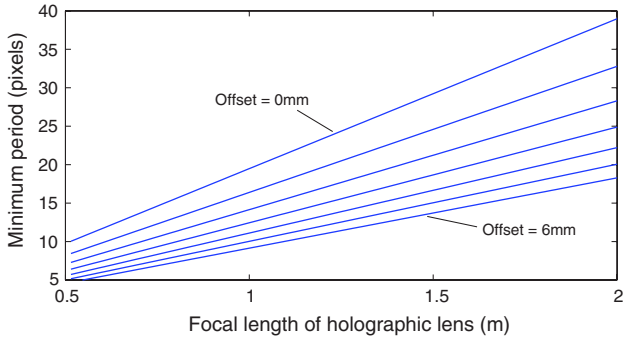

Fig. 4. (Color online) Variation in minimum local period of an on-axis lens as a function of focal length at a wavelength of 1550 nm. Pixel size is 15 μm, and lens covers 500 × 500 pixels. Curves plotted for offsets of 0, 1, 2, 3, 4, 5, and 6 mm, with period monotonically decreasing with offset.

the port spacing is 35 μm. From the perspective of our switch design it should be stressed that although this local period effect can increase the power in the $m \neq +1$ orders, the cross talk power is much less affected as it is focused away from the output plane and not coupled efficiently.

Based on the s and f parameters of our assumed system, Eq. (7) predicts that $\delta_{+1} = 0.025 \times \delta_L$. This was verified to better than 0.25% accuracy by comparing the shift in the +1 order position with the offset of the holographic lens using ray-tracing package Zemax [18]. The maximum holographic lens offset in our design example is therefore 5.6 mm for a deflection of $\delta_{+1} = 140$ μm.

To investigate the potential of this technique for fiber applications, the same Zemax model was used to analyze cross talk characteristics of the designs shown in Figs. 1(a) and 1(b). The patterns, a set of blazed gratings for the system shown in Fig. 1(a), and a set of spatially nonperiodic off-axis diffractive lenses of focal length $f_H = -1.0$m for the system shown in Fig. 1(b), were optimized for an output port separation of 35 μm. The analysis involved translating a probe fiber across the output plane, and calculating how efficiently a specific mode, m, coupled into it. The results are plotted in Fig. 5 for a system optimized to deflect the +1 order to a target position $(0, 35\,\mu\text{m})$ from the optical axis. The top and lower subplots illustrate the respective behavior of a standard and the wavefront-encoded system for modes $m = 0$, ± 1, 2, and 3. In the case of a system based on blazed gratings, each of the orders can have a coupling efficiency approaching 90%, which, due to the symmetry of the system, occurs when the test fiber is coincident with one of the output ports. In terms of the insertion loss of the signal beam, this ranges from a minimum of −0.518 dB for the port closest to the input to −0.524 dB at the fibers at the edge of the array. This finite loss is due to aberrations introduced by the nonoptimal achromatic lens used in the design, and may be reduced by using an optimized multielement lens.

In the case of a wavefront-encoded system, only the +1 order is coupled efficiently into the target fiber located 35 μm from the optical axis, with a loss of −0.602 dB. No matter the position of the test fiber, all other orders have a coupling efficiency down by at least an order of magnitude. The maximum insertion loss for the signal beam across all eight output ports was calculated to be −0.616 dB. This takes into account the effect of the incident beam no longer being parallel to the optical axis of the fiber in a defocused system, and the aberrations introduced by using the lens in a non-Fourier transform arrangement. The minimum local period occurs when we have maximum deflection ($\delta_{+1} = 140$ μm) at the corner of the hologram, and has a value of 9.9 pixels, which is greater than our 8 pixel target. In this example, wavefront encoding reduces the coupling efficiency for all $m \neq +1$ orders by at least 13.5 dB. However, the system cross talk, $\text{PC}(m, t)$, is also governed by the relative powers in the diffraction orders [Eq. (6)]. Moreover, as can be observed in the bottom subplot of Fig. 5, the beam defocus spreads the light from all the noise orders across plane F_2. Thus, the actual cross talk must be determined by coherently summing the fields of all orders, and applying a mode overlap calculation. There are several algorithms that can be used to calculate the actual replay field. In an associated publication [19] we describe how to calculate the replay field intensity and optimize the hologram pattern using the fractional Fourier transform [20]. This allows us to take into account the interference that occurs between the overlapping higher diffraction orders at the fiber plane. Figure 6 illustrates the theoretical replay field of our example system calculated using a fractional Fourier transform with $z_2 = f + 2s$, and $\delta_{+1} = 140$ μm. The figure is plotted as $10 \times \log_{10}$ (intensity), with a uniform 10% phase error applied to the off-axis lens in order to highlight the noise orders. As can be seen, all orders, bar the $m = +1$ order, are defocused, with the defocus scaling linearly with m. Moreover,

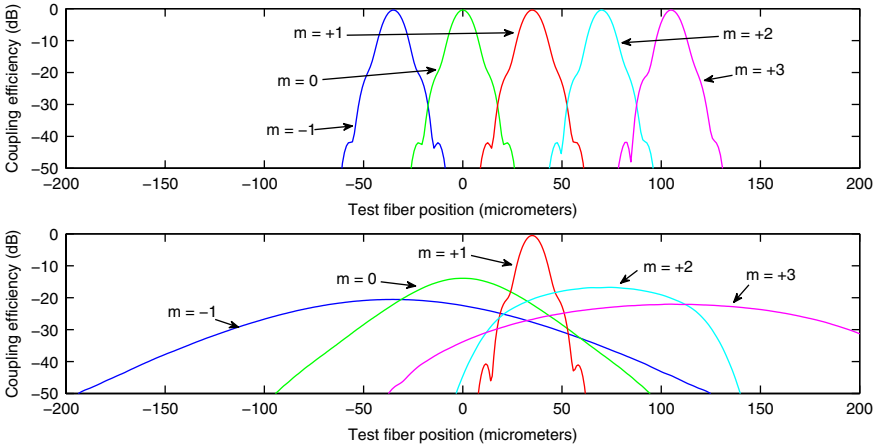

Fig. 5. (Color online) Theoretical coupling efficiency as a single-mode fiber is translated along the +1 order focal plane (plane F_1 or F_2) for diffraction orders $m = 0$, ± 1, 2, and 3. Target fiber is 35 μm from input axis. Top subplot: configuration for a Fourier-transform-based system. Lower subplot: wavefront-encoded system.

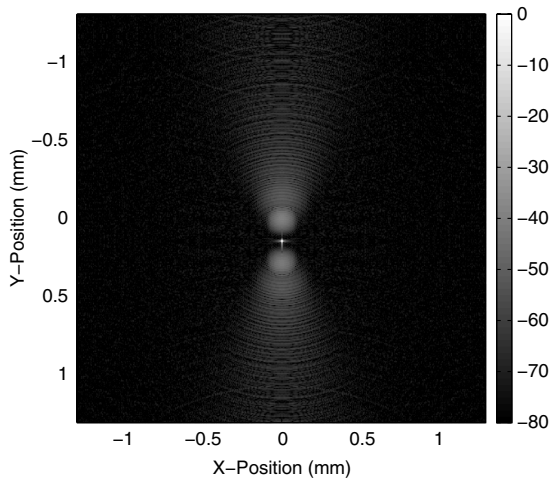

Fig. 6. Replay field at focal plane of +1 order of 500 × 500 pixel SLM displaying off-axis lens with a 10% phase error to show up higher orders. Intensity profile plotted as $10\log_{10}$ (Intensity).

interference occurs between the various orders, resulting in a ripple in the intensity distribution.

3. Application to a Free-Space Optical Interconnect

In the case of a free-space interconnect, where, for example, the output fibers of Figs. 1(a) and 1(b) are replaced by photodiodes, the situation is easier to evaluate. Here we assume that the output fibers are replaced by an array of photodetectors of dimensions $d_x \times d_y$ spaced by a distance p_d. The power captured by each detector, η_D, can be determined by simply integrating over the replay field intensity, $I(x,y)$, relative to the detector position:

$$\eta_D = \left(\frac{1}{P_T}\right)\int_{-d_x/2}^{d_x/2}\int_{-d_y/2}^{d_y/2} I(x,y)\mathrm{d}x\mathrm{d}y, \tag{8}$$

where P_T is the total diffracted power. In the case of a Gaussian beam, if the mth order is centered over a detector window, then

$$\eta_D = \frac{I_o\alpha^2\pi}{P_T}\frac{}{4}\left[\mathrm{erf}\left[\frac{d_x}{2\alpha}\right]-\mathrm{erf}\left[\frac{-d_x}{2\alpha}\right]\right]\left[\mathrm{erf}\left[\frac{d_y}{2\alpha}\right]-\mathrm{erf}\left[\frac{-d_y}{2\alpha}\right]\right]. \tag{9}$$

Here erf represents the error function [21], $\alpha = w/\sqrt{2}$, where w is the Gaussian beam radius at the detector plane, and I_o is the peak intensity. For the system shown in Fig. 1(a), w equals the radius emitted by the fiber, w_f, in the absence of aberrations. Assuming a regularly spaced array of photodetectors, higher-order diffraction orders will be centered on one or more of these elements. In the case of the system using wavefront encoding, we have an additional defocus for each order of $d(m)$, and a possible lateral offset. As stated in the previous section, the replay field can be more accurately calculated and optimized using an algorithm such as the fractional Fourier transform.

4. Experimental Validation of Wavefront Encoding

To investigate the potential of wavefront encoding, the reconfigurable optical interconnect shown in Fig. 7 was constructed. A collimated beam from a fiber-coupled 674 nm diode laser passed through a 50/50 beam splitter and was incident on a nematic LCOS SLM, assembled in-house [22], via a $4f$ relay system (lenses L_2 with $f_2 = 100$ mm and L_3 with $f_3 = 150$ mm). The SLM was optimized for 1550 nm and used a non-antireflection-coated cover plate. The device had a pixel size of 15 μm × 15 μm, with 0.5 μm dead space, and the Gaussian beam radius at the SLM plane was measured to be 2.4 mm.

Lenses L_2 and L_3 are not necessary for demonstrating the technique described in this paper, but were there for test purposes as they allowed us to control the position of the beam incident on the SLM (simultaneous translation of the lenses scanned the beam across the device while maintaininig normal incidence). However, due to the fact that $L_2 \neq L_3$, there is a demagnification of the SLM image, resulting in a scaling factor that must be applied to the defocus and offset equations. Light was diffracted by phase patterns displayed on the SLM, passed back through lenses L_3 and L_2, and 50% of this light was reflected by the 50/50 beam splitter toward the measurement arm of the system. The diffracted beams were finally focused by lens L_4 ($f_4 = 200$ mm) at the replay plane, S_R, where a rectangular aperture of dimensions 120 μm × 155 μm was used to pass one diffraction order at a time, with the 120 μm dimension of the aperture aligned parallel to the deflection axis of the grating. The patterns on the SLM were displayed across 500 × 500 pixels using 25 discrete phase levels between 0 to 2π, and the optics were arranged such that an intermediate, demagnified image of the SLM was produced at plane S_I (the intermediate SLM image). The distance from L_2 to S_I was set at f_2, while the distance from S_I to L_4 was set equal to f_4.

It should be pointed out that although the SLM used in this experiment was optimized for operation

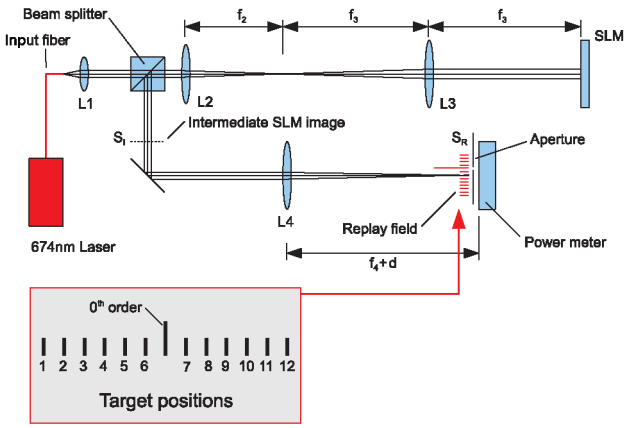

Fig. 7. (Color online) Experimental system for comparing cross talk of blazed grating and wavefront encoding schemes using visible light.

at 1550 nm, a test wavelength of 674 nm was used in our proof-of-concept experiment. The corresponding results presented in this paper provide a good indication of the ability of this technique to reduce cross talk at telecom wavelengths.

Initially, a set of blazed gratings was defined that deflected the +1 order to one of 12 target positions across the replay plane. These target positions were located at ±200, ±400, ±600, ±800, ±1000, and ±1200 μm from the optical axis. For a blazed grating, the relationship between the position of the +1 order, δ_{+1}, and period, T, is given by

$$\delta_{+1} = \frac{f_4 f_3}{f_2} \tan\left(a \sin\left(\frac{\lambda}{T}\right)\right). \tag{10}$$

The relationship between target number and physical position is given in Table 1. This relationship takes into account the effect of the relay lenses L_2 and L_3, which form a demagnified image of the SLM phase pattern at the intermediate SLM plane.

A set of wavefront-encoded holograms based on off-axis lenses was also calculated to deflect the +1 order to the same transverse positions at the aperture plane. The geometric optics design equations for the defocus of the mth order, $d(m)$, and the transverse position of the +1 order, δ_{+1}, are

$$d(m) = -\frac{f_4^2}{f_{H2}} m, \tag{11}$$

$$\delta_{+1} = \frac{\delta_{H2}}{f_4 + f_{H2}} \left(f_4 + \frac{f_4^2}{f_{H2}}\right), \tag{12}$$

where we have introduced two new terms, δ_{H2} and f_{H2}. These represent the effective focal length and lens offset of the demagnified off-axis lens at the intermediate SLM plane shown in Fig. 7, and are related to the original off-axis lens focal length, f_H, and offset, δ_H, by

Table 1. Parameters for Blazed Grating and Wavefront-Encoded Patterns

		Blazed Grating	Wavefront-Encoded
Position	δ_{+1} (μm)	Period, T, in pixels	Offset, δ_H, in pixels
1	−1200	−11.23	−266.7
2	−1000	−13.48	−222.2
3	−800	−16.85	−177.8
4	−600	−22.47	−133.3
5	−400	−33.70	−88.9
6	−200	−67.40	−44.4
7	+200	+67.40	+44.4
8	+400	+33.70	+88.9
9	+600	+22.47	+133.3
10	+800	+16.85	+177.8
11	+1000	+13.48	+222.2
12	+1200	+11.23	+266.7

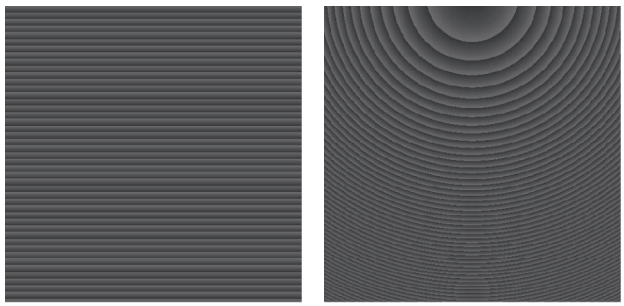

(a) (b)

Fig. 8. Phase patterns used on the LCOS device: (a) Blazed grating (covers whole of device); (b) wavefront-encoded pattern (500 × 500 pixels).

$$f_{H2} = \left(\frac{f_2}{f_3}\right)^2 f_H \tag{13}$$

and

$$\delta_{H2} = \frac{f_2 \delta_H}{f_3}. \tag{14}$$

For this test the pattern was simply defined as an off-axis lens of focal length $f_H = 1.0$ m offset by the distance specified in Eq. (12). Thus, taking into account the relay system lenses, L_2 and L_3, the demagnification of the original SLM kinoform pattern increases the defocus to $f_{H2} = 0.444$ m. This resulted in the replay plane for the +1 order being shifted toward L_4 by a distance, $d(+1) = 90$ mm.

The typical quantized phase patterns displayed on the SLM (shown as bitmaps) for the blazed grating and wavefront-encoded patterns are illustrated in Figs. 8(a) and 8(b). Figures 9(a) and 9(b) show the associated replay fields recorded using a CCD camera. As can be seen from Fig. 9(a), in the case of a Fourier plane system, all the diffraction orders are focused at the same plane. In the case of the wavefront-encoded system, only the +1 order is focused at the replay plane, all the other orders are strongly defocused, as shown in Fig. 9(b). It should also be noted that a spurious reflection from one of the components in the test rig can be observed to the right of the diffraction orders in Fig. 9(a), but is not observable in Fig. 9(b) due to the introduced defocus.

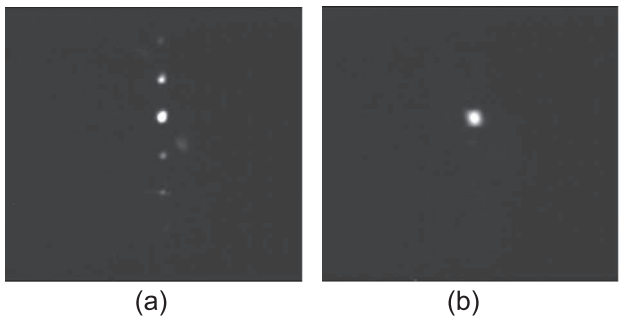

(a) (b)

Fig. 9. Intensity images of the replay planes at 674 nm: (a) Blazed grating; (b) wavefront encoded. The images were taken at the same laser power and at the same magnification.

Table 2. Cross Talk Matrix (in Decibels) for Blazed Grating Patterns[a]

		Target Position											
	(dB)	1	2	3	4	5	6	7	8	9	10	11	12
Measurement Position	1	0.00	−33.49	−35.23	−38.51	−38.56	−32.62	−35.00	−39.30	−40.25	−43.50	−42.46	**−24.30**
	2	−34.82	0.00	−33.45	−35.04	−35.59	−32.32	−35.69	−39.66	−41.44	−42.49	**−25.31**	−44.84
	3	−38.92	−34.12	0.00	−33.22	−35.03	−31.71	−35.00	−37.92	−40.62	**−26.32**	−43.13	−37.70
	4	**−16.88**	−37.93	−35.34	0.00	−34.27	−30.99	−34.64	−42.05	**−25.96**	−42.80	−43.31	−30.03
	5	**−25.74**	−39.24	**−17.71**	−33.75	0.00	**−29.58**	−36.00	**−26.17**	−40.71	−30.58	−43.31	−33.01
	6	−33.62	−30.65	**−29.53**	**−26.09**	**−17.02**	0.00	**−25.72**	−30.42	−32.91	−34.04	−36.72	−37.46
	7	−36.95	−35.86	−34.00	−33.66	**−29.20**	−24.86	0.00	**−17.43**	**−24.77**	**−27.85**	−31.86	−34.86
	8	−32.39	−43.18	−30.82	−40.25	**−26.35**	−32.49	−31.02	0.00	−31.49	**−17.32**	−38.18	**−26.40**
	9	−29.59	−42.66	−43.59	**−26.98**	−38.95	−32.28	−34.25	−34.27	0.00	−33.21	−36.28	**−17.92**
	10	−37.58	−43.89	**−26.30**	−40.54	−38.69	−32.22	−34.85	−37.63	−33.80	0.00	−33.48	−36.97
	11	−42.92	**−24.22**	−40.37	−40.28	−40.11	−32.70	−35.11	−38.39	−38.55	−35.85	0.00	−33.80
	12	**−24.36**	−41.14	−43.65	−40.89	−41.57	−32.62	−34.17	−38.98	−40.34	−38.61	−34.86	0.00

[a]Bold denotes cross talk values > -30 dB.

In order to deflect the light to the required location in the standard $2f$ system, an aperiodic blazed grating was designed using a modulo 2π algorithm [7] and downloaded onto the SLM. Experimentally, the diffraction efficiency for all 12 positions was measured to be $86.5 \pm 4.0\%$. The cross talk at each target location was also measured as the SLM was cycled to deflect the $+1$ order to all 12 target positions, giving a 12×12 power matrix with cross talk values ranging from −44.85 to −16.9 dB. The high upper cross talk level is due to phase quantization errors and pixel edge effects producing a nonideal phase pattern. The theoretical spot size at the replay plane was calculated using Gaussian beam theory to be 26.8 μm, and measured using a CCD camera to be 31 μm. This discrepancy was attributed to experimental error and system aberrations. Using Eq. (9) for our given aperture size, the clipping loss is only 0.01%. Table 2 lists the measured signal/cross talk matrix for this measurement. From this table we can see that symmetry exists in the distribution of the high cross talk positions. For example, in all cases a strong cross talk power appears at the symmetric −1 order position as shown by the central diagonal line.

For the wavefront-encoded patterns, the test aperture was moved to the shifted focal plane, and the measurements repeated using exactly the same aperture dimensions. Note that the aperture was translated in this plane to the same target positions. The efficiency of the 12 test wavefront-encoded patterns was measured to be $88.4 \pm 2.8\%$, with the cross talk ranging from −44.1 to −28.7 dB. Table 3 lists the corresponding signal/cross talk matrix. Across the table we observe just two cases where the cross talk is above −30 dB. A comparison of the insertion loss is shown in Fig. 10, showing the power diffracted into the $+1$ order when it was deflected to the 12 target positions using either the blazed grating or the wavefront-encoded patterns. There is actually a slight improvement in diffraction efficiency with the wavefront-encoded holograms. This is possibly due to a slight error in the position of the test aperture with respect to the two replay planes.

The theoretical (calculated using a Gaussian beam model) and measured Gaussian beam radii at plane S_R were 27.8 and 39.5 μm, respectively. This 27% increase in spot size at wavelength 674 nm is attributed to the difficulty in displaying the higher spatial frequencies of a wavefront-encoded pattern

Table 3. Cross Talk Matrix (in Decibels) for Wavefront-Encoded Holograms[a]

		Target Position											
		1	2	3	4	5	6	7	8	9	10	11	12
Measurement Position	1	0.00	−32.98	−34.37	−33.18	−33.44	−31.47	−35.13	−36.84	−40.23	−41.46	−43.02	***−41.11***
	2	***−34.13***	0.00	−32.73	−32.20	−33.54	−31.53	−34.92	−37.47	−40.14	−41.46	***−42.67***	−42.75
	3	***−36.92***	−34.43	0.00	−31.93	−32.23	−31.16	−34.95	−37.07	−39.97	***−41.20***	−44.03	−42.55
	4	−32.78	−34.26	−32.58	0.00	−30.94	−30.95	−34.41	−36.98	***−39.40***	−41.07	−42.20	−42.63
	5	−36.92	−34.77	***−32.67***	**−28.68**	0.00	**−28.87**	−33.60	***−37.32***	−39.63	−40.84	−43.81	−42.44
	6	−39.10	−37.10	***−35.11***	***−31.65***	***−30.55***	0.00	***−31.33***	−35.44	−38.89	−40.20	−41.64	−42.72
	7	−41.34	−39.46	−37.61	−33.78	***−32.41***	***−31.27***	0.00	***−30.68***	***−33.73***	***−35.63***	−37.09	−38.53
	8	−41.60	−39.63	−37.51	−33.10	***−33.58***	−30.59	−31.98	0.00	−31.69	***−33.17***	−35.36	***−35.84***
	9	−41.22	−39.08	−38.12	***−33.61***	−33.38	−31.80	−34.18	−33.75	0.00	−34.50	−34.78	***−35.44***
	10	−41.34	−39.23	***−36.88***	−34.12	−33.54	−31.60	−34.66	−36.63	−35.82	0.00	−34.37	−37.02
	11	−40.97	***−39.23***	−38.12	−33.98	−33.75	−31.06	−34.77	−36.98	−38.83	−35.70	0.00	−33.98
	12	***−40.86***	−39.23	−37.77	−33.39	−33.48	−31.83	−34.52	−37.22	−39.79	−40.18	−36.14	0.00

[a]Bold italic denotes the high cross talk high values of Table 2 that are now < -30 dB. Bold denotes cross talk values > -30 dB.

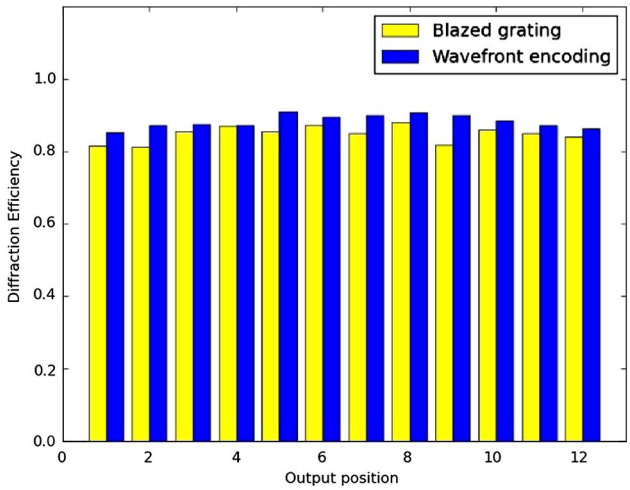

Fig. 10. (Color online) Diffraction efficiency to all target positions for a blazed grating (yellow), and an equivalent wavefront-encoded pattern (blue).

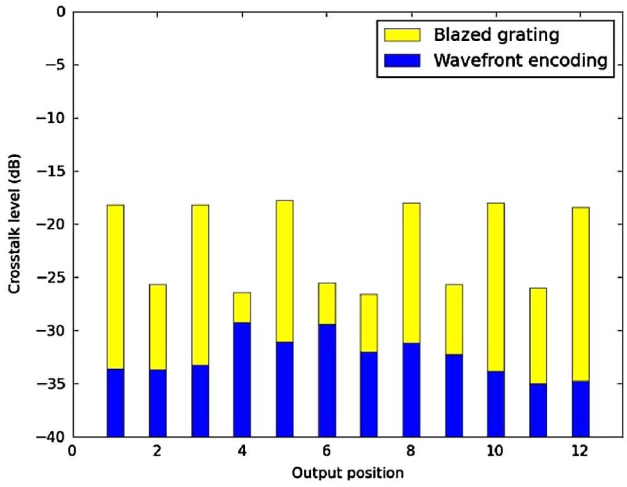

Fig. 12. (Color online) Maximum cross talk at each of the 12 target positions for a standard blazed grating and the wavefront-encoded pattern.

on the LCOS SLM, and interference between the various off-axis lens diffraction orders at the output plane. Again, using Eq. (9) for our given aperture size, the clipping loss is only 0.25%.

The minimum local period occurs when we have maximum deflection of the target beam ($\delta_{+1} = 1.2$ mm), and has a value of 5.2 pixels. Thus, although both the theoretical example of Section 2 and the experiment described have the same focal length and value for N_{SLM}, and require approximately the same maximum holographic lens offset, due to the fact that we are using a shorter wavelength, the experimental system requires a much smaller local period. As a result, the 1550 nm system described in Fig. 1(b) will not be as affected by quantization effects as our experimental system, and the spot size should be closer to the value predicted using Gaussian beam propagation theory. In addition, as we used an SLM optimized for 1550 nm for this test, the effects of interpixel field fringing would have been more pronounced than for a thinner cell SLM optimized for 674 nm.

Figure 11 illustrates the cross talk for a sample deflection position (position 12). There is suppression of the cross talk power (light unintentionally deflected to position 12 when the SLM is configured to deflect light to another position) when we use a wavefront-encoded system in all but one of the cases (when the target is position 2). We observe that the cross talk suppression, defined as the difference between the worst-case blazed grating performance and wavefront-encoded system performance, is much greater than 10 dB.

Figure 12 is the key result of this paper as it shows the worst-case cross talk values at each test position for both the blazed grating patterns and the equivalent wavefront-encoded patterns, and illustrates that cross talk is always suppressed when defocusing is applied. Experimentally the wavefront-encoded system has a maximum cross talk 12.6 dB lower than that of the equivalent blazed grating pattern.

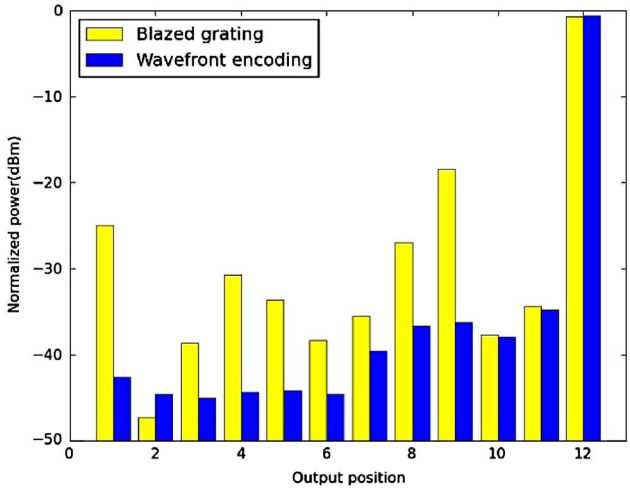

Fig. 11. (Color online) Measured performances (signal and cross talk). This typical result was taken at location 12, with the SLM cycling through all 12 blazed grating and wavefront-encoded patterns.

5. Conclusions

Initial tests have shown that by using wavefront encoding based on an offset defocusing lens instead of a conventional grating, we can reduce the worst-case cross talk by over an order of magnitude (12.6 dB) in a reconfigurable LCOS-SLM-based beam steering switch. Preliminary verification of this technique at 674 nm used a free-space optical setup. The measured maximum cross talk level we achieved was −28.7 dB, with no impact on efficiency and uniformity. This technique works by purposefully building an aberration into the optical system and displaying an optimized hologram that ensures only the signal beam is optimally coupled. In the case of wavefront encoding based on the simplest aberration defocusing, the holograms took the form of off-axis lenses.

The performance of wavefront encoding using defocusing depends on the practical limits of displaying offset lens functions on the SLM. It was observed that the focused spot broadened by 27.3% at 674 nm. This discrepancy between theoretical and measured spot size is primarily attributed to the difficulty in displaying the higher spatial frequencies of a wavefront-encoded pattern and interference between the various orders at the output plane. It should be noted that we used a nonoptimized device in this experiment. The SLM was designed for use at 1550 nm and tested at 674 nm. If the SLM were tested in a telecom system operating at the longer wavelength of 1550 nm, the minimum local period would increase, while interpixel effects would remain constant, thereby allowing a more accurate hologram to be displayed. Minimization of this spot broadening effect using optimized holograms, and the ultimate optical scalability of this approach are currently being investigated, particularly with regards to the trade-off between the focal length applied to the SLM and fiber switch insertion loss. Further reductions in cross talk will require careful control of the amount of power in the zeroth and higher orders, which will be aided by using an antireflection-coated SLM cover plate.

Future work will be directed to the development of a fiber switch using this approach, and into investigating wavefront encoding techniques other than defocus. This includes the use of astigmatism in switches that employ cylindrical optics, and in the use of matched spatial filters incorporated with lenslet arrays before the fiber array. Efforts can also be made toward the generation of integrated phase profiles combining hologram and wavefront encoding together. As described in a related article [19], using a fractional Fourier transform to calculate the replay field allows us to directly use algorithms such as the Gerchberg–Saxton routine [23] in the design of the holograms.

This work was supported by the Cambridge Integrated Knowledge Centre (CIKC), by the UK Engineering and Physical Sciences Research Council (EPSRC) platform grant (Liquid Crystal Photonics) and follow on fund (ACCESS project), and by the Research Councils UK (RCUK) Global Uncertainties program.

References

1. M. C. Wu, O. Solgaard, and J. E. Ford, "Optical MEMS for lightwave communication," J. Lightwave Technol. **24**, 4433–4454 (2006).
2. D. T. Neilson, R. Frahm, P. Kolodner, C. A. Bolle, R. Ryf, J. Kim, A. R. Papazian, C. J. Nuzman, A. Gasparyan, N. R. Basavanhally, V. A. Aksyuk, and J. V. Gates, "256 × 256 port optical cross-connect subsystem," J. Lightwave Technol. **22**, 1499–1509 (2004).
3. W. A. Crossland, I. G. Manolis, M. M. Redmond, K. L. Tan, T. D. Wilkinson, M. J. Holmes, T. R. Parker, H. H. Chu, J. Croucher, V. A. Handerek, S. T. Warr, B. Robertson, I. G. Bonas, R. Franklin, C. Stace, H. J. White, R. A. Woolley, and G. Henshall, "Holographic optical switching: the ROSES demonstrator," J. Lightwave Technol. **18**, 1845–1854 (2000).
4. C. Uche, B. Fracasso, W. A. Crossland, J. L. de Bougrenet de la Tocnaye, and T. D. Wilkinson, "Development of large capacity and low-crosstalk holographic switches using LCOS spatial light modulators," Ferroelectrics **278**, 219–226 (2002).
5. E. Hallstig, L. Sjoqvist, and M. Lindgren, "Intensity variations using a quantized spatial light modulator for non-mechanical beam steering," Opt. Eng. **42**, 613–619 (2003).
6. L. Xu, J. Zhang, and L. Y. Wu, "Influence of phase delay profile on diffraction efficiency of liquid crystal optical phased array," Opt. Laser Technol. **41**, 509–516 (2009).
7. M. Johansson, S. Hård, B. Robertson, I. Manolis, T. Wilkinson, and W. Crossland, "Adaptive beam steering implemented in a ferroelectric liquid crystal spatial-light-modulator free-space, fiber-optic switch," Appl. Opt. **41**, 4904–4911 (2002).
8. K. L. Tan, S. T. Warr, I. G. Manolis, T. D. Wilkinson, M. M. Redmond, A. A. Crossland, R. J. Mears, and B. Robertson, "Dynamic holography for optical interconnections II. Routing holograms with predictable location and intensity of each diffraction order," J. Opt. Soc. Am. A **18**, 205–215 (2001).
9. A. G. Georgiou, M. Komarcevic, T. D. Wilkinson, and W. A. Crossland, "Hologram optimisation using liquid crystal modelling," Mol. Cryst. Liq. Cryst. **434**, 183–198 (2005).
10. J. E. Stockley, D. Subacius, and S. A. Serati, "The influence of the interpixel region in liquid crystal diffraction gratings," Proc. SPIE **3635**, 127–136 (1999).
11. M. A. A. Neil, M. J. Booth, and T. Wilson, "New modal wavefront sensor: a theoretical analysis," J. Opt. Soc. Am. A **17**, 1098–1107 (2000).
12. D. G. Leyva, B. Robertson, T. D. Wilkinson, and C. J. Henderson, "Aberration correction in an adaptive free-space optical interconnect with an error diffusion algorithm," Appl. Opt. **45**, 3782–3792 (2006).
13. P. M. Blanchard and A. H. Greenaway, "Simultaneous multiplane imaging with a distorted diffraction grating," Appl. Opt. **38**, 6692–6699 (1999).
14. D. Marcuse, "Loss analysis of single-mode fiber splices," Bell Syst. Tech. J. **56**, 703–718 (1977).
15. D. G. Leyva, B. Robertson, C. J. Henderson, T. D. Wilkinson, A. C. O'Brien, and G. Faulkner, "Cross-talk analysis in a telecentric adaptive free-space optical relay based on a spatial light modulator," Appl. Opt. **45**, 63–75 (2006).
16. E. Noponen, J. Turunen, and A. Vasara, "Electromagnetic theory and design of diffractive-lens arrays," J. Opt. Soc. Am. A **10**, 434–443 (1993).
17. M. J. Yzuel, J. Campos, A. Márquez, J. C. Escalera, J. A. Davis, C. Iemmi, and S. Ledesma, "Inherent apodization of lenses encoded on liquid-crystal spatial light modulators," Appl. Opt. **39**, 6034–6039 (2000).
18. Zemax, Radiant ZEMAX LLC.
19. B. Robertson, Z. Zhang, H. Yang, M. M. Redmond, N. Collings, J. Liu, R. Lin, A. M. Jeziorska-Chapman, J. R. Moore, W. A. Crossland, and D. P. Chu are preparing a manuscript to be called, "Application of the fractional fast Fourier transform to the design of LCOS based optical interconnects and fiber switches," to be submitted to Applied Optics (2011).
20. H. M. Ozaktas, *The Fractional Fourier Transform: with Applications in Optics and Signal Processing* (Wiley, 2001).
21. M. Abramowitz and I. A. Stegun, *Handbook of Mathematical Functions* (Dover, 1965), Chap. 7.
22. Z. Zhang, A. M. Jeziorska-Chapman, N. Collings, M. Pivenko, J. Moore, B. Crossland, D. P. Chu, and B. Milne, "High quality assembly of phase-only liquid crystal on silicon (LCOS) devices," J. Displ. Technol. **7**, 120–126 (2011).
23. R. W. Gerchberg and W. O. Saxton, "A practical algorithm for the determination of the phase from image and diffraction plane pictures," Optik **35**, 237–246 (1972).